Power to Fuels: Dynamic Modeling of a Slurry
Bubble Column Reactor in Lab-Scale for Fischer

applied sciences

MDPI

Article

Power to Fuels: Dynamic Modeling of a Slurry Bubble Column Reactor in Lab-Scale for Fischer Tropsch Synthesis under Variable Load of Synthesis Gas

Siavash Seyednejadian [1,*], Reinhard Rauch [2], Samir Bensaid [1], Hermann Hofbauer [3], Gerald Weber [4] and Guido Saracco [1]

1 Department of Applied Science and Technology, Politecnico di Torino, Corso Duca degli Abruzzi 24, 10129 Torino, Italy; samir.bensaid@polito.it (S.B.); guido.saracco@polito.it (G.S.)
2 Engler-Bunte-Institut, Karlsruher Institute of Technology, Engler-Bunte- Ring 3, 76139 Karlsruhe, Germany; reinhard.rauch@kit.edu
3 Institute of Chemical Engineering, Technical University of Vienna, Getreidemarket 9/166, 1060 Vienna, Austria; hermann.hofbauer@tuwien.ac.at
4 Institute Bioenergy 2020+, Wiener Strasse 49, 7540 Güssing, Austria; gerald.weber@bioenergy2020.eu
* Correspondence: siavash.seyednejadian@polito.it; Tel.: +39-011-090-4662

Received: 23 February 2018; Accepted: 25 March 2018; Published: 28 March 2018

Abstract: This research developed a comprehensive computer model for a lab-scale Slurry Bubble Column Reactor (SBCR) (0.1 m D_t and 2.5 m height) for Fischer–Tropsch (FT) synthesis under flexible operation of synthesis gas load flow rates. The variable loads of synthesis gas are set at 3.5, 5, 7.5 m^3/h based on laboratory adjustments at three different operating temperatures (483, 493 and 503 K). A set of Partial Differential Equations (PDEs) in the form of mass transfer and chemical reaction are successfully coupled to predict the behavior of all the FT components in two phases (gas and liquid) over the reactor bed. In the gas phase, a single-bubble-class-diameter (SBCD) is adopted and the reduction of superficial gas velocity through the reactor length is incorporated into the model by the overall mass balance. Anderson Schulz Flory distribution is employed for reaction kinetics. The modeling results are in good agreement with experimental data. The results of dynamic modeling show that the steady state condition is attained within 10 min from start-up. Furthermore, they show that step-wise syngas flow rate does not have a detrimental influence on FT product selectivity and the dynamic modeling of the slurry reactor responds quite well to the load change conditions.

Keywords: Power to Liquid; Fischer–Tropsch; dynamic modeling; lab-scale

1. Introduction

In the last decade, Carbon Capture Utilization (CCU) with the aid of Renewable Energy Source (RES) power has led to significant progress in the field of Power to Gas (PtG) and Power to Liquid (PtL) technologies. In order to reduce Greenhouse Gas (GHG) emissions, European Energy policy proposes that the share of renewable energy is 40% by 2020 and 80% by 2050 [1]. This electricity-to-fuel process stabilizes the electrical power grid by converting the fluctuating characteristics of Renewable Energy Sources into storable energy carrier e.g., gaseous hydrocarbons (H_2 or CH_4) in PtG. This process may also provide liquid fuel for the use of chemicals and transport in PtL technology [2]. In this respect, Power to Liquid is a strong candidate for the transformation of power into chemical electricity as there is no loss during long-term storage; it has wide-ranging applications in the transport sector, due to its

high energy density which is compatible with existing infrastructures [3]. The main pathway in this transformation is *Fischer–Tropsch Synthesis*, which offers many advantages in the process design and for optimizing product selectivity. The feedstock of the FT process is attained using generated synthesis gas and steam/co-electrolysis can be employed for generating syngas out of water and carbon dioxide. This enables RES power to be coupled with electrolysis providing a carbon free cycle [4]. Other alternatives for syngas generation include biomass gasification and natural gas reforming. Syngas derived from autothermal reforming or gasification technology with an air separation unit must be employed in large scale FT facilities and those methods have the further benefit of generating a high syngas ratio (H_2/CO) [5]. However, CO_2 gasification using biomass technology is not able to provide a sufficient syngas ratio for producing liquid fuel. Therefore, steam electrolysis or a water gas shift reactor could be used for adjusting the H_2/CO ratio so that it is equal to 2 (usage syngas ratio) [6].

In the field of power to fuel technology, flexible analysis of a Low Temperature Fischer–Tropsch (LTFT) reactor under variable operating conditions presents more challenges compared to other value-added processes such as methanation and the Dimethyl ether process. These challenges involve more complexity in FT product selectivity and lower feasibility in the dynamic analysis of an LTFT reactor compared to methanation and the DME synthesis [7]. In this respect, the most suitable FT reactors for analyzing under flexible operation are the Multi-Tubular Fixed Bed Reactor and the Slurry Bubble Column Reactor. In the Fixed Bed Reactor (FBR), dynamic analysis addresses the feasibility of reducing the size of H_2 storage and optimizing the temperature profile along the catalyst bed [8], whereas, in the FT Slurry type, the analysis is focused on improving mass transfer phenomena (gas-to-liquid contact and interfacial mass transfer area), leading to enhanced selectivity and catalyst performance with regard to complex hydrodynamic features and scale up issues [9]. During recent years, the Slurry Bubble Column Reactor has been identified as the best option for Fischer–Tropsch synthesis due to its many advantages compared to the other reactors. These advantages include (1) flexible temperature control and excellent heat transfer; (2) efficient inter-phase contacting which results in higher productivity; (3) low pressure drop leading to reduced compression costs; (4) better use of catalyst surface (fine particles less than 100 μm) allowing suitable liquid-solid mass transfer [5,10].

However, this reactor presents several technical challenges in the design of the pilot plant as well as large scale due to following reasons: (1) potential formation of slug regime flow; (2) very little information on mass transfer data; (3) difficulty in scale up due to complex hydrodynamic features; (4) Obstacles to the separation of fine catalysts from the slurry phase.

This work focuses on the dynamic modeling of a Slurry Bubble Column Reactor for Fischer Tropsch synthesis in pilot plant scale under variable loads of synthesis gas. This transient calculation is performed in once-through conditions under a cobalt-supported catalyst to identify *the effect of load change conditions* on FT selectivity, CO conversion, the alpha value and temperature distribution of the slurry reactor in the Winddiesel Technology. Winddiesel technology developed by the Technical University of Vienna has already been tested at an FT demonstration plant based on synthesis gas from biomass steam gasification and steam electrolysis in cases of availability of renewable energy [11,12]. In the modeling of the Fischer–Tropsch Slurry Bubble Column reactor (FT-SBCR) in lab-scale, a set of appropriate hydrodynamic parameters is incorporated into coupled FT kinetics and mass transfer through MATLAB code. This new approach enables us to analyze the behavior of *all species* through the length of the reactor from start-up to steady state condition. Moreover, in this dynamic modeling, change in the superficial gas velocity due to chemical reaction is coupled to the set of PDEs using *the overall species transport equations*. This approach estimates the reliable calculation of the gradient of gas flow rate for bubbles which proposes a realistic prediction of the reactor performance [13]. However, the majority of slurry reactors models for superficial gas velocity within the reactor linearize the gas velocity with syngas conversion [14–16].

In dynamic modeling SBCR for FT process, a number of methodologies based on several well-developed hydrodynamic concepts such as the Axial dispersion model (ADM), Single bubble class (SBC), two bubble class (TBC), etc. with different FT kinetics have been proposed. In 2002, J.W.A

de Swart and R. Krishna [14] developed a model to predict the steady state and dynamic behavior of a bubble column slurry reactor for Fischer Tropsch synthesis. Their numerical procedure was based on four partial differential equations solved using Method Of Lines (MOL). The results indicated that steady-state is achieved within about seven minutes from start-up and no thermal runways were observed in a reactor of commercial scale. Furthermore, the influence of the back-mixing of the liquid phase on hydrogen conversion for two different reactor diameters (1, 7.5 m) was compared. It was concluded that at 1 m diameter the axial dispersion coefficient decreased, leading to a flatter velocity profile in the liquid phase, which in turn results in higher conversions of hydrogen [14].

In 2005, Rados et al. [13] simulated an FT-SBCR with two chemical reaction systems. They analyzed the hydrodynamic behavior of two bubble class models by assuming linear first-order reaction kinetics. They also considered the influence of the Axial Dispersion Model (ADM) on conversion and reactor diameter and compared this effect in ideal reactors i.e., plug flow (PF) and completely stirred tank (CST) [13]. In 2009, Hooshyar et al. [15] developed a dynamic slurry FT for both single and double bubble class at churn turbulent flow regime. They concluded that there is no discrepancy between single and double class models in terms of concentration, temperature and conversion profile. Thus, they considered the single bubble class as a less complex reliable model to analyze the slurry bubble column reactors [15]. In 2008, Laurent Sehabiague [17] et al. developed a computer model for a large-scale FT slurry reactor. The simulator was used to optimize superficial gas velocity and reactor geometry for producing 10,000 (barrels/day) of liquid fuels. Different operating conditions were also used to find the maximum space time yield (STY). However, the condition for maximum productivity was considered as the optimum operating condition because of lower operating and capital cost [17].

Accordingly, almost all dynamic modeling of FT slurry reactors has focused on the commercial scale of slurry bubble column reactors and there has been no detailed transient computer model at pilot scale (reactor diameter < 1 m) for SBCR so far. In fact, the modeling of laboratory scale FT slurry is a more difficult task because of the wealth of dynamic features, such as the prediction of rise velocity of small bubbles and wall effects, which make hydrodynamic parameters quite sensitive to system properties, and the presence of impurities [18]. Thus, the present work investigates, for the first time, the transient analysis of a slurry FT reactor in lab-scale under supported catalyst cobalt for all key components of Fischer–Tropsch synthesis developed by a MATLAB code. This comprehensive modeling enables us to predict the behavior of several slurry reactor parameters such as CO conversion, FT selectivity, α-value and temperature profile under variable loads of synthesis gas. Furthermore, the results of the modeling are in good agreement with the experimental data. The experimental data is adopted from a Master of Science thesis which was conducted using the Fischer–Tropsch research plant. The plant is located in town of Güssing in Austria [11,12]. Appendixs A and B reflect the experimental measurements for both base load (syngas flow rate of 5 m^3/h) and change load conditions (syngas flow rate of 3.5 m^3/h and 7.5 m^3/h) in one specific run [12].

2. Fischer–Tropsch Reaction Scheme

Fischer–Tropsch synthesis consists of a set of polymerization reactions leading to a blend of linear paraffins of different carbon numbers. In the present investigation, the rate expression of Fischer–Tropsch synthesis under catalyst cobalt is employed based on Yates and Satterfield 1991 [19] (see the relation of reaction kinetics in Table 1). In this reaction kinetics ($-R_{co}$), by modifying parameters a and b, the model predictions of CO conversion correspond to the experimental measurements. Anderson-Schulz Flory model gives an indication of the distribution for n-paraffins based on their mass fraction (W_n) which can be expressed with the relation of ASF distribution of products as mentioned in Table 1 (W_n relation). W_n is defined by parameter α (Chain growth probability factor). In fact, α-value reflects the distribution of the weight percentage of products with regard to their carbon number [20]. Factor α strongly depends on temperature, pressure and the catalyst used in the process. Generally, in our model, alpha correlation is employed in terms of temperature as

mentioned in the relation of chain growth probability factor (Table 1), which is described by Song et al. (2004) [21]. In the section of model comparison, in order to calculate α-value a semi-logarithmic plot of mass fraction against carbon number is considered (logarithmic relation in Table 1) producing a straight line. The slope of the line is given the α-value. The calculation is performed for different operating conditions based on both model and experimental data. The products of Fischer–Tropsch synthesis under catalyst cobalt are predominantly paraffins through the generic reaction in Table 1 (paraffin reaction form). Therefore, the rate of paraffin formation based on Anderson-Sculz-Flory (ASF) equation can be calculated from r_i relation in Table 1 [22]. Also, Table 2 illustrates the operating conditions and several lab parameters. Details of the FT reactor and experimental setup are mentioned in references [11,12].

Table 1. Kinetic Characteristics of Fischer–Tropsch Slurry Bubble Column reactor (FT-SBCR): reaction parameters, product distribution.

Reaction Characteristics	Relations	Constants, Parameters and Paraffin Reaction Form	
Reaction Kinetics	$-R_{co} = \frac{a\, P_{co} P_{H_2}}{(1+bP_{co})^2}$	$a = 1.59064 \times 10^{-12}$ $b = 7.99389 \times 10^{-6}$	
Chain grow probability factor (Song et al.)	$\alpha = \left(A\frac{y_{co}}{y_{H_2}+y_{co}} + B\right)[10.0039(T-533)]$	$A = 0.2332$ $y_{co} = 0.2$	$B = 0.633$ $y_{H_2} = 0.4$
Anderson Sculz-Flory distribution of products.	$W_n = n\,(1-\alpha)^2.\alpha^{n-1}$	$\log\frac{W_n}{n} = n\log(\alpha) + \log\frac{(1-\alpha)^2}{\alpha}$	
Rate of paraffin formation based on ASF distribution.	$r_i = R_{co}\alpha^{n-1}$	$n\,CO + (2n+1)H_2 \rightarrow C_nH_{2n+2} + nH_2O$	

Table 2. Operating conditions and liquid properties of lab-scale Fischer–Tropsch Slurry Bubble Column.

Operating Condition	
Reactor Temperature	503 K
Reactor Pressure	20 bar
H_2/CO	2
Reactor diameter	0.1 m
Reactor height	2.5 m
Volumetric Flow Rate (loads)	3.5, 5, 7.5 m^3/h
Liquid Phase Properties	
Liquid Density	715 kg/m^3
Surface tension	0.023 N/m
Liquid Viscosity	3×10^{-3} Pa.s

3. Modeling Activity

3.1. Model Framework

A detailed computer model for a pilot plant FT-SBCR (D = 0.1 m, H = 2.5 m) for all the key components of FT synthesis reactor was developed. A set of Partial Differential Equations (PDEs) of transport species including mass transfer and kinetics was successfully coupled with hydrodynamic parameters. In general, 10 equations for the gas phase (single bubble class) and 10 equations for the liquid phase need to be solved simultaneously. The reactor model was established with these assumptions: (1) an Axial Dispersion Model (ADM) in the form of a convection-diffusion phenomenon with a single class of gas bubble diameter is considered (ADM-SBCD); (2) the gas-liquid mass transfer resistance is positioned on both the gas and liquid side; (3) based on the non-dimensional form of Peng-Robinson equation-of-state (PR-EOS), the compressibility factor of the gas phase corresponds to near unity ($Z \approx 1$). The PR-EOS is a suitable fluid model for FT systems to predict vapor-liquid

compositions and flow rates inside the slurry reactor [23,24]; (4) considering a low pressure drop in the slurry reactor, the operating pressure is assumed to be constant along the reactor height; (5) the reactor operates under isothermal condition; (6) by assuming constant pressure and temperature, the overall continuity balance occurs at the inlet and outlet of the reactor (Equation (3)); (7) liquid-solid mass transfer resistance may be ignored and consequently solid suspension in liquid is simulated as a single pseudo-homogeneous slurry phase in this work; (8) chemical reaction through Langmuir Hinshelwood Hougen Watson (LHHW) kinetics in liquid phase is considered.

Based on these model assumptions, the mass balances of each component in gas and liquid phases can be derived as follows:

Gas phase equations:

$$\underbrace{\frac{\partial\left(\varepsilon_g C_{g,i}\right)}{\partial t}}_{\text{Accumulation}} = \underbrace{\frac{\partial}{\partial z}\left(D_g\ \varepsilon_g \frac{\partial C_{g,i}}{\partial z}\right)}_{\text{Axial Dispersion}} - \underbrace{\frac{\partial}{\partial z}\left(\varepsilon_g U_g C_{g,i}\right)}_{\text{Convection}} - \underbrace{\left(K_l a\right)_{g,i}\varepsilon_l\left(\frac{C_{g,i}}{A_i} - C_{l,i}\right)}_{\text{Mass Transfer}} \quad (1)$$

Liquid phase equations:

$$\underbrace{\frac{\partial(\varepsilon_l C_{l,i})}{\partial t}}_{\text{Accumulation}} = \underbrace{\frac{\partial}{\partial z}\left(\varepsilon_l D_{ax,l}\frac{\partial C_{l,i}}{\partial z}\right)}_{\text{Axial Dispersion}} - \underbrace{\frac{\partial}{\partial z}(\varepsilon_l U_l C_{l,i})}_{\text{Convection}} + \underbrace{\left(K_l a\right)_{g,i}\varepsilon_l\left(\frac{C_{g,i}}{Ai} - C_{l,i}\right)}_{\text{Mass Transfer}} - \underbrace{\varepsilon_l \rho_{cat}\varepsilon_{cat} r_i}_{\text{Reaction}} \quad (2)$$

Total concentration:

$$\sum_i^n C_{g,i} = C_{tot,in} = \frac{P}{ZRT} = C_{tot,out} \quad (3)$$

In the above equations, A_i denotes the Henry's constant (H_i) for syngas and light hydrocarbons (CO, H_2, H_2O, C_1 and C_2). By employing Henry's law solubility factor ($P_i = x_i \times H_i^{\infty}$), the Henry's constant for each reactant gas was calculated based on the heat of solution for each component and operating temperature [25].

$$A_i = H_i/RT \quad (4)$$

$$H_i = H_i^* \exp\left(-\frac{\Delta H_{s,i}}{RT}\right) \quad (5)$$

where, the value of parameters H_i^* and $\Delta H_{s,i}$ are listed in reference [25].

For heavier components (C_4^+), Ai was calculated using Raoult's law for gas-liquid phase at the equilibrium as follows:

$$A_i = {}^{H_i^{\infty}}/_{RT}.1/_{C_{tot}^L} \quad (6)$$

$$C_{tot}^L = {}^{\rho_L}/_{MW_{L,avg.}} \quad (7)$$

where, C_{tot}^L is the total concentration of liquid components, ρ_L is the liquid density, $MW_{L,avg.}$ is the average molecular weight of liquid components and H_i^{∞} is the Henry's constant at infinite dilution which is defined as follow:

$$H_i^{\infty} = \gamma_i^{\infty}\ P_{i,sat} \quad (8)$$

where γ_i^{∞} is the activity coefficient for heavier components and $P_{i,sat}$ is the vapor pressure of component i which is calculated from asymptotic behavior correlations (extension of the Antoine equations). By supposing ideal behavior of FT mixture due to long-chain n-paraffins, the Henry's constant for the mixture can be expressed by:

$$\mathrm{Ln}H_{i,mix}^{\infty} = \sum_j x_j \mathrm{Ln}\ H_j^{\infty} \quad (9)$$

where j is the components in the solvent. Since LnH_i^{∞} and $Ln\gamma_i^{\infty}$ is asymptotically linear with solute carbon number (m), the formula for calculating the infinite-dilution activity coefficient becomes as follow:

$$Ln\gamma_m^{\infty} = Ln\gamma_r^{\infty}\frac{(n-m)}{(n-r)} \tag{10}$$

where n is the carbon number of solvent (n-paraffin) and r denotes the carbon number of reference solute (n-C_6H_{14}) in the same solvent. They are described in more detail in references [24,26].

As mentioned in the model assumption, since the reactor is supposed to be operated under constant pressure and temperature, the total concentration is constant. As a consequence, the variation of the gas flow rate due to chemical reaction and mass transfer is determined by assuming the constant total concentration of components in single bubble gas diameter (Equation (3)). Therefore, the Equation (11) as a sub-model in the form of a gas state equation is incorporated into the SBCD model. This sub-model used for behavior of superficial gas velocity inside the reactor is a reliable approach since it considers the concentrations of all gaseous components [13].

$$\frac{\partial U_g}{\partial z} = -\frac{1}{C_{tot}}\sum_{i=1}^{n} K_l \times a \times \varepsilon_l \times \left(\frac{C_{g,i}}{A_i} - C_{l,i}\right) \tag{11}$$

Table 3 depicts the initial and boundary conditions of Equations (1), (2) and (11). The initial values in the model are set based on pressure, temperature and concentration of species. The boundary conditions adopted from Danckwerts' type are defined for the gas and liquid at the inlet and outlet of the reactor. For the gas phase at the reactor inlet, the concentration is taken from a syngas composition under the operating conditions of the laboratory, calculated based on Table 3. The inlet superficial gas velocity for single bubble gas diameter is calculated from Equation (14).

The effective gas-liquid interfacial area for mass transfer of small bubbles between two phases can be expressed as follows [27]:

$$a = 6 \times \varepsilon_g / d_B \tag{12}$$

The mass transfer coefficient (K_l) is calculated from the following empirical correlation. It is applicable in a wide range of operating conditions which leads to a good prediction of gas-liquid mass transfer [27]:

$$K_l a = 1.77 \times \sigma^{-0.22} \times \exp(1.65U_l - 0.65\mu_l) \times \varepsilon_g^{1.2} \tag{13}$$

Table 3. Initial and boundary conditions for the slurry reactor model.

Initial Condition (t = 0)	Reactor Inlet (z = 0)	Reactor Outlet (z = H)
$C_{gi} = C_{gi,in}$	$C_{gi} = C_{gi,in}$ $C_{g,i0} = \frac{P_i}{ZRT}$	$\frac{\partial C_{g,i}}{\partial z} = 0$
$C_{li} = C_{gi,in}/A_i$	$\varepsilon_l D_l\left(\frac{\partial C_{l,i}}{\partial z}\right)_{z=0} = U_l\left(C_{l,i} - C_{g,i0/A_i}\right)$	$\frac{\partial C_{g,i}}{\partial z} = 0$
$U_i = U_{g,in}$	$U_{gi} = U_{g,in}$	$\frac{\partial U_g}{\partial z} = 0$

The superficial gas velocity is defined as the volumetric gas flow rate divided by the cross-sectional area of the reactor above the gas distributor [28]:

$$U_{g,in} = \frac{V_f}{A_r} \tag{14}$$

The initial bubble size depending on buoyancy forces and surface tension is derived by the theoretical Davidson and Schuler expression [29]:

$$d_B = \left[\frac{6\sigma\, d_0}{g\,(\rho_{SL} - \rho_G)}\right]^{1/3} \quad (15)$$

The gas hold up can be expressed as the volume of the gas phase divided by the reactor volume consisting of gas volume, liquid volume and volume of catalyst used [28]:

$$\varepsilon_g = \frac{V_{gas}}{V_{gas} + V_{liquid} + V_{cat}} \quad (16)$$

This is calculated to be 0.161 ($m^3_G\ m^{-3}_R$) and the catalyst volume fraction (ε_{cat}) is calculated to be 0.34 ($m^3_{cat}\ m^{-3}_L$). It should be noted that in the Equations (1) and (2), ε_L is the liquid holdup ($m^3_L\ m^{-3}_R$) and r_i denotes reaction rate of FT species ($mol\ kg^{-1}_{cat}\ s^{-1}$). Moreover, the velocity of liquid inside the reactor is assumed to be 0.00089 m/s.

In the slurry bubble column reactors, the gas bubble coalescence occurs in a short time with an increase of the column diameter, and the large bubbles collect around the center of the column in the operation of a churn turbulent regime. This is called heterogeneous flow, which usually occurs when the superficial gas velocity is greater than 0.05 m/s. When the gas-liquid mixture reaches the surface, the bubbles disengage, allowing the degassed liquid to recirculate. Therefore, the main cause of back-mixing and liquid dispersion in the lab-scale slurry FT reactor is attributed to downward velocity of the liquid in the wall region and upward direction ($V_L(r)$) in the central axis [30]. Based on Riquarts correlation [31] the magnitude of $V_L(0)$ depends on the column diameter, superficial gas velocity and kinematic viscosity of the liquid phase as described in Equation (17). The experimental data [30,31] show that the liquid phase axial dispersion coefficient ($D_{ax,L}$) has a direct proportionality to column reactor diameter and centre-line liquid velocity as mentioned in Equation (18).

$$V_L(0) = 0.2 \times (g\,D_t)^{1/2} \times (U^3_{g,in}/g\,\nu_L)^{1/8} \quad (17)$$

$$D_{ax,L} = 0.31 \times V_L(0) \times D_t \quad (18)$$

According to reference [30,31], the two correlations given above are the most appropriate ones for the estimation of axial dispersion coefficient which was recommended in all systems (including slurry). The axial dispersion coefficient of the gas phase for the small bubbles is equal to that of the liquid phase according to the relationship which was proposed by Sehabiague et al. [10].

3.2. Computer Solution Procedure

In this transient calculation, a MATLAB pdepe (Partial Differential Equations Parabolic Elliptic) solver is implemented. The solver converts a set of PDEs to ODEs (Ordinary Differential equations) using an accurate spatial discretization based on a specified grid size. The solution domain is equal to the length scale of the reactor and the optimized discretization is chosen based on a balance between the desired level of accuracy and the affordable CPU time [8].

For solving equations, the mass balance of 10 components of H_2, CO, H_2O, CO_2, CH_4, C_2H_6, C_4H_{10}, $C_{10}H_{22}$, $C_{18}H_{38}$, and $C_{30}H_{62}$ in two phases, gas and liquid, are considered.

4. Results and Discussions

The simulation of the FT slurry reactor begins with the start-up after all heating devices are switched on and the alarm values are set. Once an operating parameter such as temperature or pressure, attains its alarm value, the research plant is automatically switched off and this is called an alarm shut down (ASD). The alarm values are vitally important since they ensure a safe operation of the plant. Then, the FT plant is started under N_2 flow as an inert gas in the manual mode until the FT reactor reaches a temperature of 453 K, at which the wax in the FT reactor is liquid. Afterwards, the plant is switched to the automatic mode and the FT reactor reaches the required operating temperature of

503 K and the plant starts to operate under syngas. The time required for the start-up stage before switching the plant to automatic mode is about 2–3 h.

4.1. Species Distribution

4.1.1. The Behavior of Components H_2, CO

Firstly, the aforementioned hydrodynamic parameters are implemented in the computer model then the equations related to small bubbles of gas species and the liquid phase are coupled to obtain the concentration behavior of all FT key components from the beginning to the steady state conditions through the length of the reactor. As Figure 1 shows, at $\tau = 0$ there is no carbon monoxide and hydrogen in either of the two phases. At normal operation ($\tau > 0$), these species enter the reactor with their own inlet values (which are already calculated based on the boundary conditions in Table 3; $C_{g,in}$), initiating the reaction. At the reactor inlet a maximum value is seen and liquid is supposed to be saturated with gas phase. The CO and H_2 are consumed due to the chemical reaction and their concentration decreases across the reactor length to the equilibrium values in two phases. In this respect, "wall effects" cause small bubbles to dissolve faster into the liquid phase before reaching steady state values. The concentration behavior of species (mol/m^3_{gas} for gaseous components and mol/m^3_{liquid} for liquid components) shows that the steady state values are reached at 10 min, as expected from the experimental data [12]. The CO conversion in this base load condition equals 58%, which is slightly overestimated compared to the experimental data. The run is performed for T = 503 K, P = 20 bar, U_g = 0.17 m/s, ε_{cat}= 0.34.

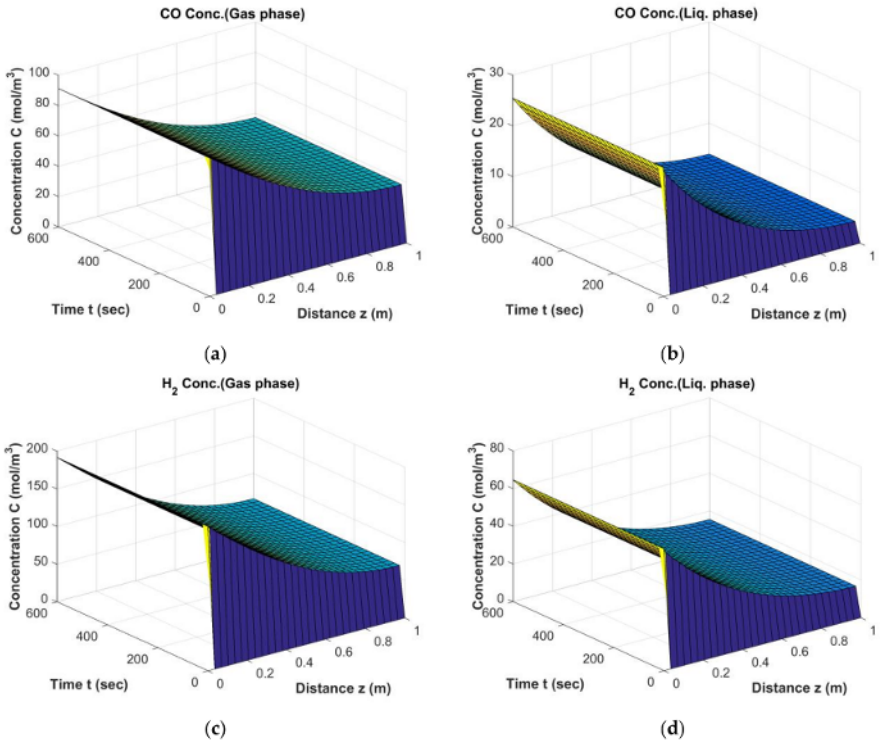

Figure 1. Results of Fischer–Tropsch (FT) Simulation; The behavior of CO, H_2 in gas phase (**a**,**c**) and liquid phase (**b**,**d**) from start-up to steady state conditions (D_t = 0.1 m, H = 2.5 m, ε_{cat} = 0.34, $U_{g,in}$ = 0.17 m/s).

4.1.2. The Behavior of Components H_2O, CO_2

As Figure 2 illustrates, water vapor, which is one of the products of FT synthesis, increases over the reactor height and over the time. Since the FT reaction occurs under a co-supported catalyst,

no water gas shift reaction is promoted and the inlet CO_2 acts as an inert through the process. The CO_2 concentration increases due to the volume reduction of off-gas and syngas consumption. It is worth noting that the presence of diluents such as CO_2, CH_4 or N_2 has a beneficial influence in slurry bubble column reactors. The inert (here as carbon dioxide) enables supplementary mixing energy to the slurry system to maintain catalyst suspension. On the other hand, in FBRs we need to avoid diluents since they elevate the pressure drop across the reactor bed [32].

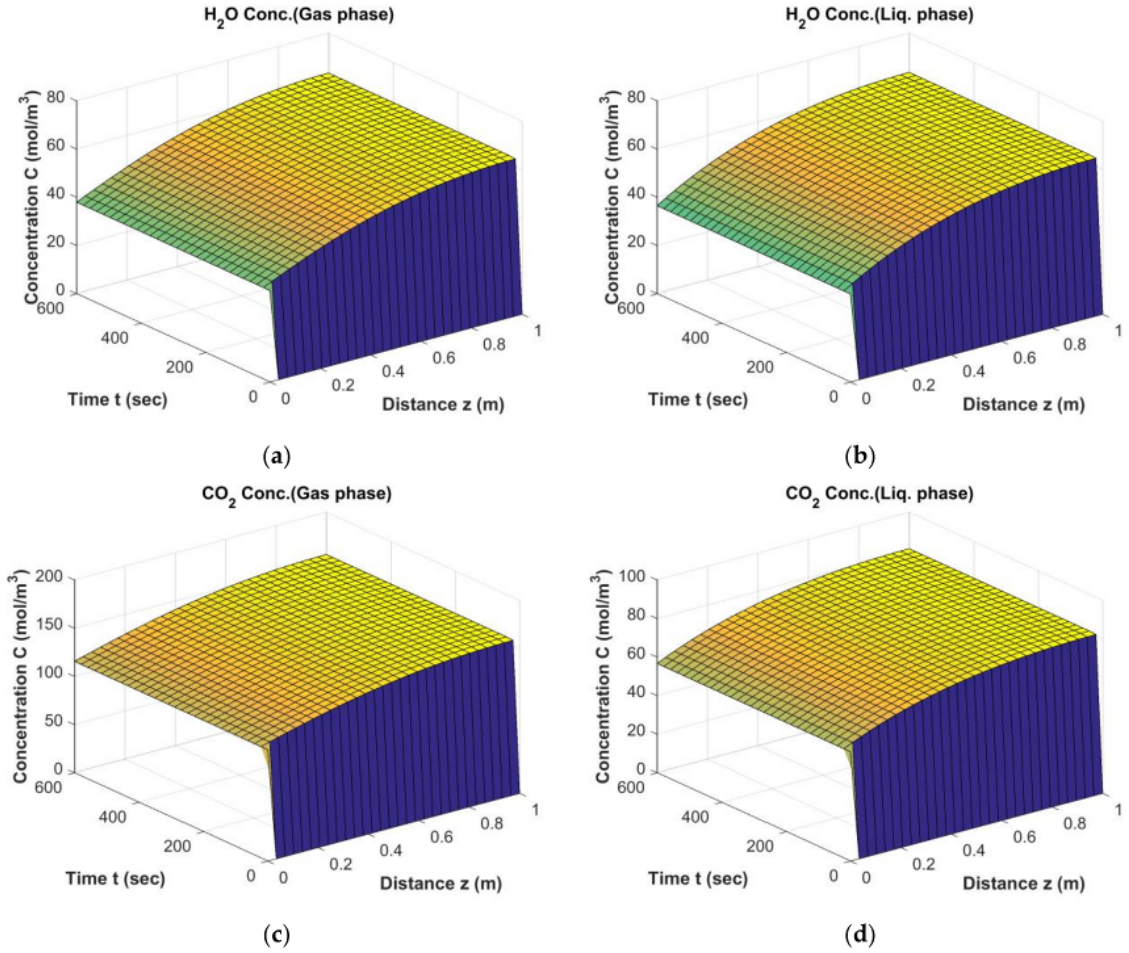

Figure 2. Results of FT Simulation; The behavior of H_2O and CO_2 in gas phase (**a**,**c**) and liquid phase (**b**,**d**) from start-up to steady state conditions (D_t = 0.1 m, H = 2.5 m, ε_{cat} = 0.34, $U_{g,in}$ = 0.17 m/s).

4.1.3. The Behavior of Components CH_4, C_2H_6, C_4H_{10}

Methane, ethane and butane increase over time and achieve their highest concentration at the final time in the reactor outlet. These highest values in the gas phase reach around 85, 35 and 50 mol/m^3 for CH_4, C_2H_6 and C_4H_{10}, respectively as shown in Figure 3.

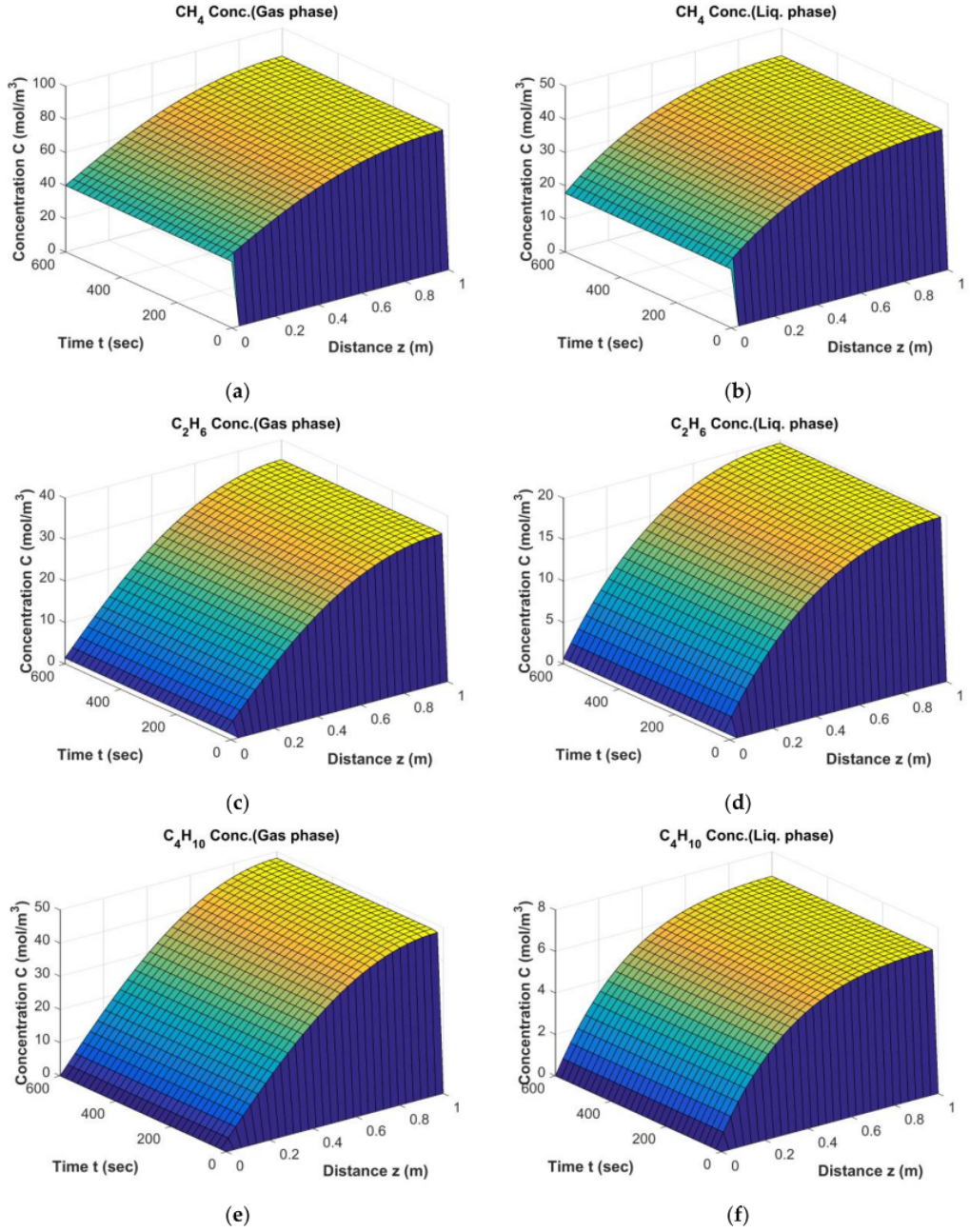

Figure 3. Results of FT Simulation; The behavior of CH_4, C_2H_6 and C_4H_{10} in gas phase (**a**,**c**,**e**) and liquid phase (**b**,**d**,**f**) from start-up to steady state conditions (D_t = 0.1 m, H = 2.5 m, ε_{cat} = 0.34, $U_{g,in}$ = 0.17 m/s).

4.1.4. The Behavior of Liquid Products $C_{10}H_{22}$, $C_{18}H_{38}$, $C_{30}H_{62}$

In this mathematical modeling, three components are considered as representatives of each specific carbon cut. $C_{10}H_{22}$, $C_{18}H_{38}$ and $C_{30}H_{62}$ were introduced as naphtha, diesel and wax respectively, which are derived from three condensers with reaction water in each condenser and collected in each related drum [12]. The results of modeling show that all three sets of products have a similar profile through the slurry reactor. As illustrated in Figure 4, the liquid products have an upward trend over time through the reactor height and the highest magnitude belongs to the middle distillate whereas diesel and wax stand at lower values respectively.

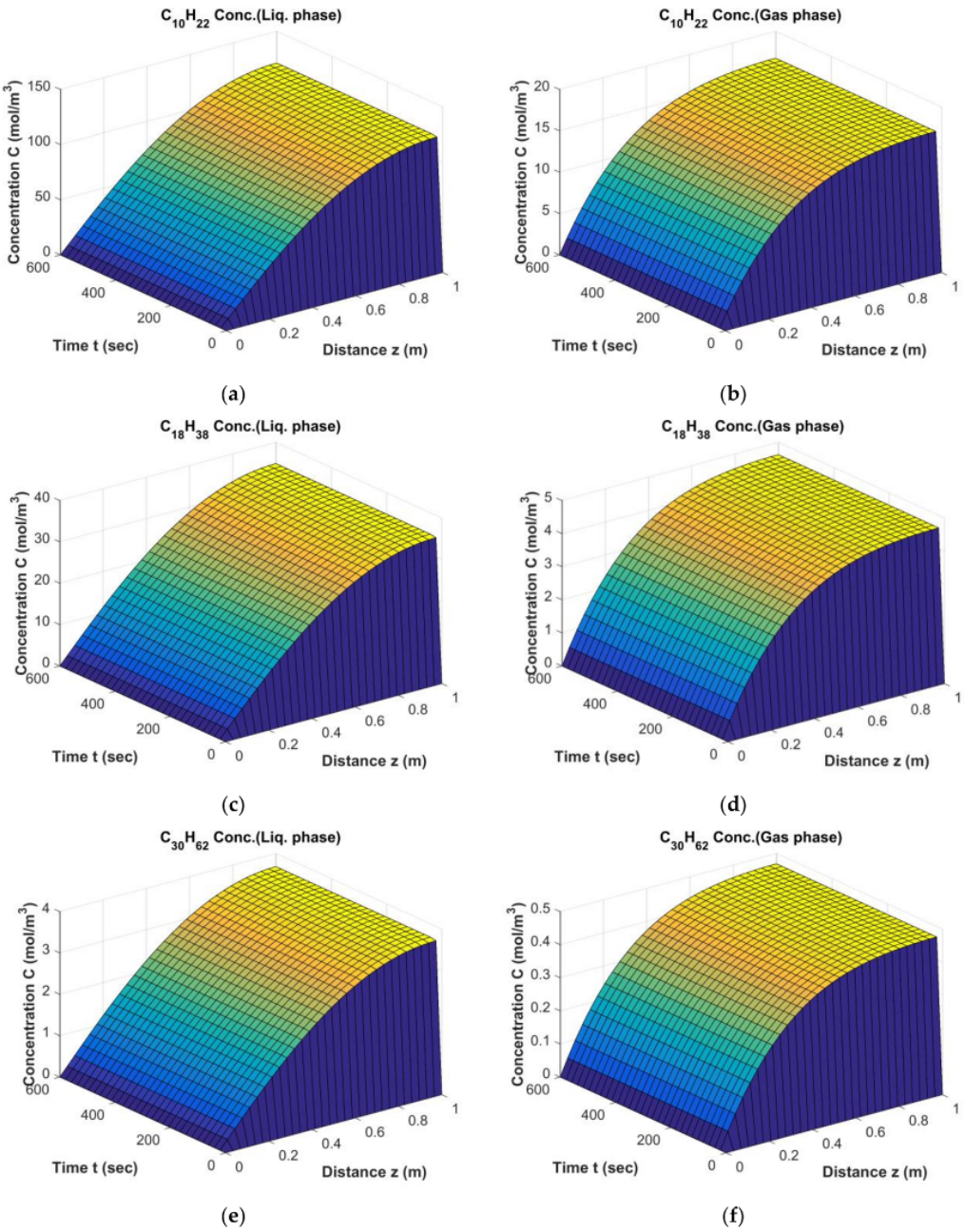

Figure 4. Results of FT simulation; The behavior of $C_{10}H_{22}$, $C_{18}H_{38}$ and $C_{30}H_{62}$ in liquid phase (**a**,**c**,**e**) and gas phase (**b**,**d**,**f**) from start-up to steady state conditions (D_t = 0.1 m, H = 2.5 m, ε_{cat} = 0.34, $U_{g,in}$ = 0.17 m/s).

These simulations results relate to base load conditions (volumetric gas flow rate 5 m^3/h). The computer model is also able to work quite well under variable loads of synthesis gas. Therefore, the flow rate in the model was changed in the range of 3.5–7.5 m^3/h to find maximum CO conversion and FT product selectivity.

4.2. Model Comparison with Experimental Data

The comparison of the model results with experimental data was conducted based on the composition (volume %) of syngas and off-gas which were measured by a GC device under base load and change load conditions. Figures 5–7 show a comparison of the predicted values by the computer

model with the measured data from the conducted experiments. In general, the results show that the predicted model is in good agreement with the experimental data. When compared with FT products only in the case of naphtha (C_8–C_{10}) is there a noticeable difference between model and laboratory data in all three operating conditions. This is due to the volatility of this carbon cut and difficulty in collecting them together. In product distribution (Figures 5c, 6c and 7c) only, two groups (C_8–C_{15}) and (C_{30}–C_{40}) show a deviation as well as discontinuities in the model prediction. The deviation is probably due to the neglect of olefin formation in the reactor modeling and the discontinuities can be attributed to the model equations which were solved for specific classes of FT species (C_1, C_2, C_4, C_{10}, C_{18} and C_{30}). As mentioned earlier, the α-value can be derived from the slope of the drawn line in all three load conditions. In the model, the α-value for volumetric flow rate of 3.5, 5 and 7.5 m^3/h is calculated to be 0.89, 0.9 and 0.88 respectively. It shows that change load conditions have almost no influence on the α-value or catalyst selectivity as predicted from the experiment.

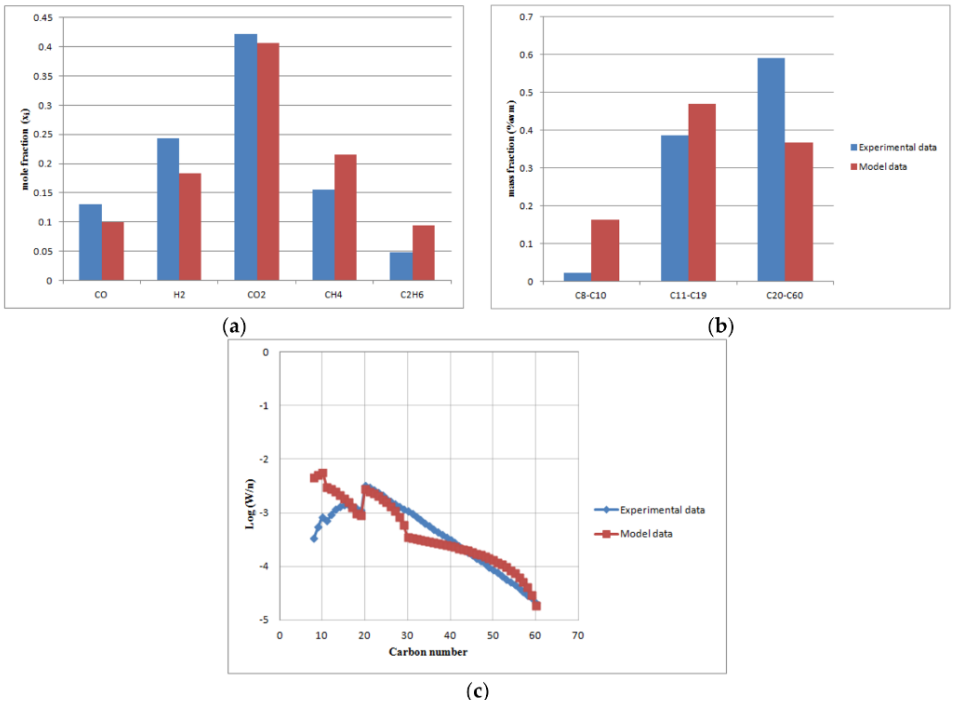

Figure 5. The comparison of the predicted model with experimental data at base load conditions (volumetric gas flow rate 5 m^3/h, T = 503 K, ε_{cat} = 0.34, P = 20 bar): (**a**) off-gas molar fractions; (**b**) FT products (naphta, diesel, wax); (**c**) ASF distribution.

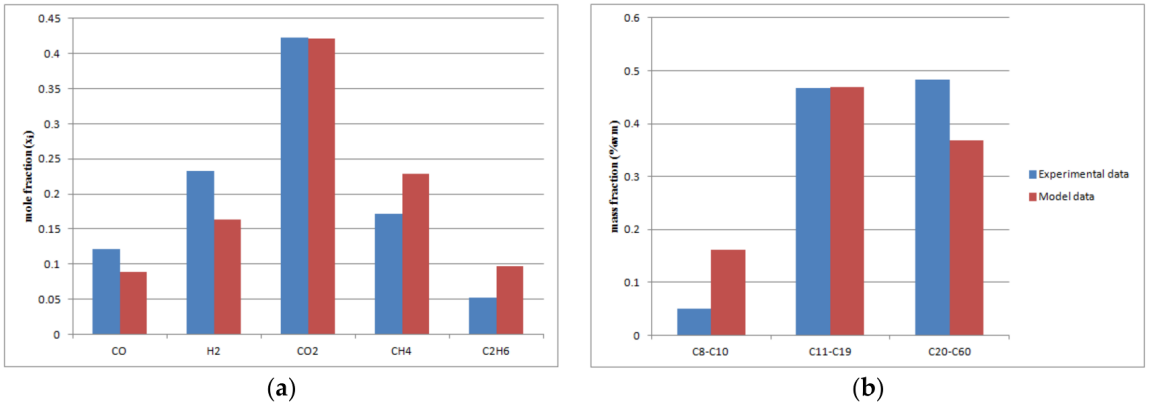

Figure 6. *Cont.*

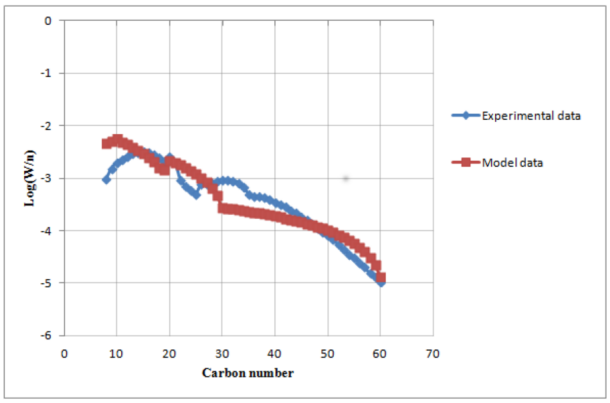

(**c**)

Figure 6. The comparison of the predicted model with experimental data at change load conditions (volumetric gas flow rate 3.5 m^3/h, T = 503 K, ε_{cat} = 0.34, P = 20 bar): (**a**) off-gas molar fractions; (**b**) FT products (naphta, diesel, wax); (**c**) ASF distribution.

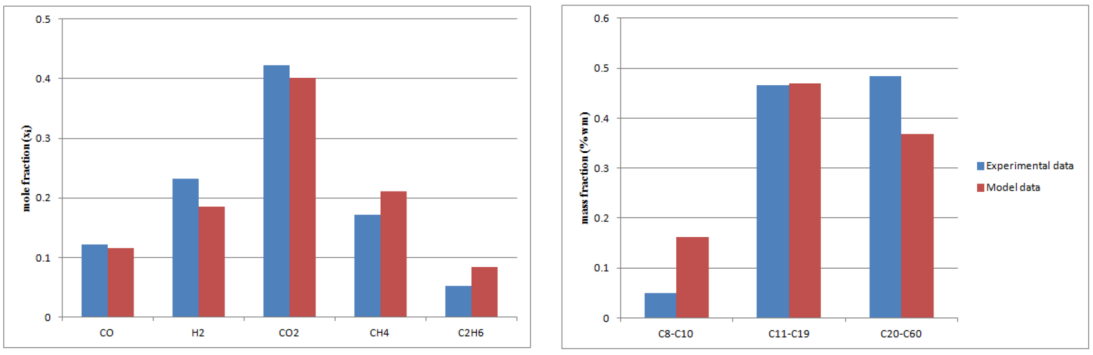

(**a**) (**b**)

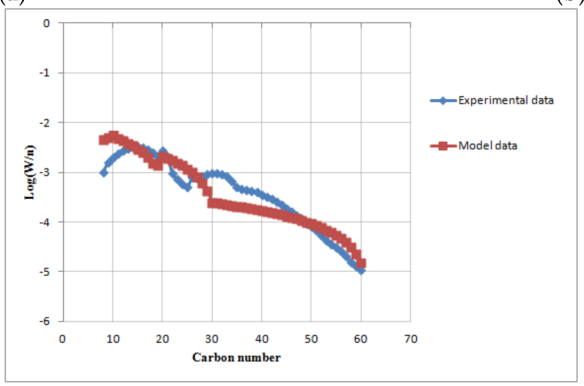

(**c**)

Figure 7. The comparison of the predicted model with experimental data at change load conditions (volumetric gas flow rate 7.5 m^3/h, T = 503 K, ε_{cat} = 0.34, P = 20 bar): (**a**) off-gas molar fractions; (**b**) FT products (naphtha, diesel, wax); (**c**) ASF distribution.

The results show that the CO conversion both in the model and experiments has lower values at a higher superficial velocity of syngas. This is due to the decreasing residence time of reactants at higher values of velocity. Thus, the maximum CO conversion occurs at 3.5 m^3/h which is equal to 60%. As Figure 8 shows, the CO conversion also is in good agreement with the experimental data; however, the model values are slightly overestimated. This is due to larger area for gas-liquid mass transfer in the result of the assumption of the single bubble class diameter.

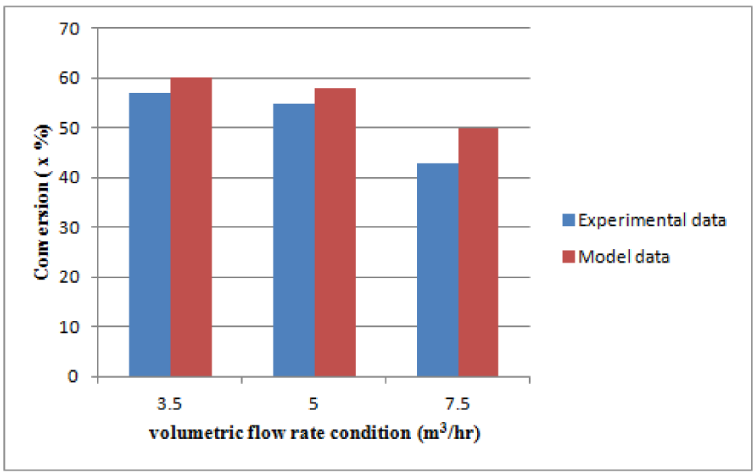

Figure 8. CO Conversion at base and change load condition based on experimental and model data.

4.3. The Effect of Temperature on Product Selectivity

One strength of FT reactor modeling is that analysis of the product selectivity with reaction temperatures can be carried out to find the desired operating conditions. Figures 9–11 illustrate the variation of product selectivity based on mass fraction with operating temperature at three loads of volumetric flow rates (3.5, 5, 7.5 m^3/h), respectively. As shown in these figures, for all three loads with increasing temperature the light gaseous (C_1–C_4), naphtha (C_5–C_{10}) and diesel increase whereas, heavier liquid fuels such as wax (C_{20}–C_{60}) tend to decrease. This trend can be expected since higher temperatures tend to shift the α-parameter to lower values thus producing more light hydrocarbons (C_1–C_4). In the design of the lab-scale SBCR for the FT process, it is advisable to operate the reactor under a narrow temperature range (483–503 K). This prevents catalyst deactivation, avoiding higher increases in methane as well as obtaining selectivity of diesel products [12].

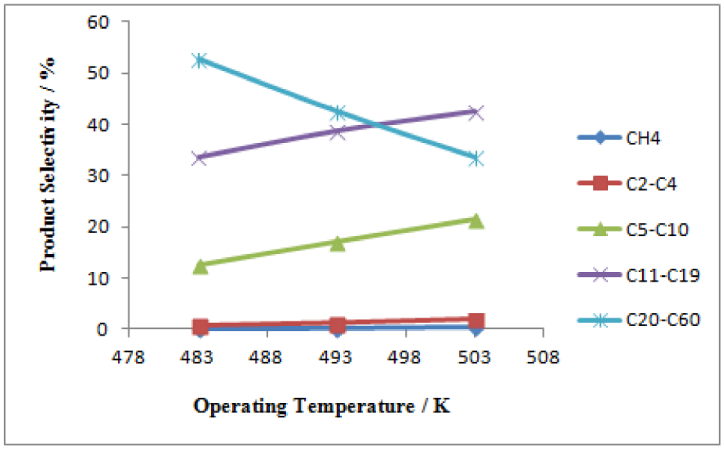

Figure 9. Influence of operating temperature on product selectivity; D_t = 0.1 m, H = 2.5 m, V_f = 3.5 m^3/h, P = 20 bar, ε_{cat} = 0.34.

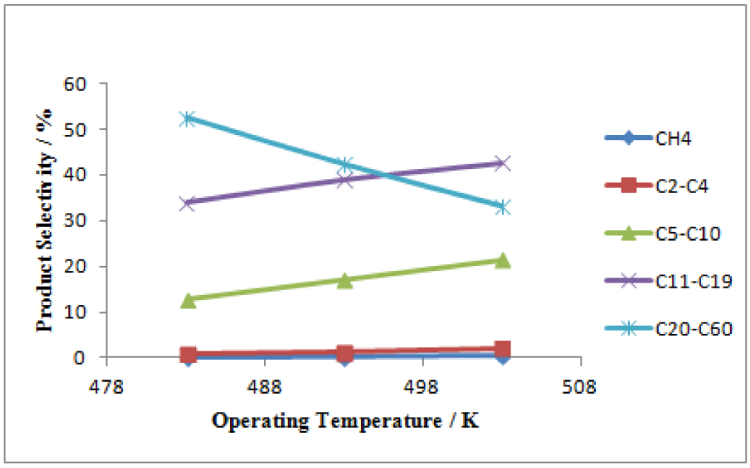

Figure 10. Influence of operating temperature on product selectivity; D_t = 0.1 m, H = 2.5 m, V_f = 5 m^3/h, P = 20 bar, ε_{cat} = 0.34.

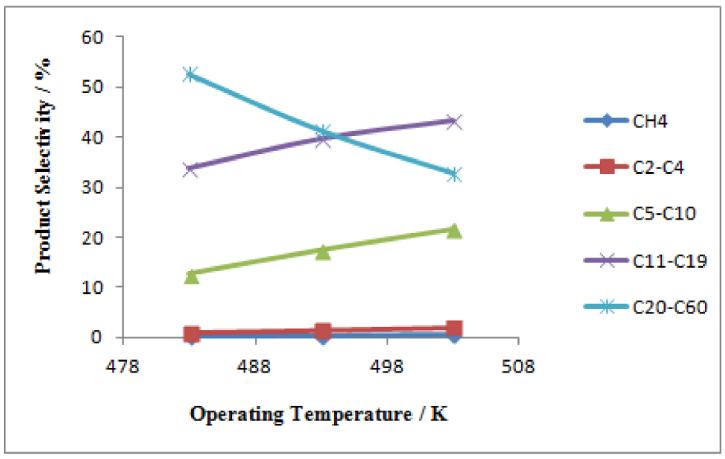

Figure 11. Influence of operating temperature on product selectivity; D_t =0.1 m, H = 2.5 m, V_f = 7.5 m^3/h, P = 20 bar, ε_{cat} = 0.34.

It was concluded that by increasing the load of syngas flow rate, the selectivity of wax and diesel remain constant in each corresponding temperature. It was also concluded that there is a homogenous temperature profile within the reactor.

4.4. The Behavior of the Species Inside the Reactor

The experimental data of the research FT reactor in laboratory scale is only able to reflect information about the reactor outlet. However, this mathematical modeling attempts to predict the dynamic behavior of the system through the height of the reactor which includes the concentration change of all species along the reactor length. Figure 12a,b show the molar concentration and conversion of syngas (CO and H_2) along the reactor bed at base load condition, respectively. The slightly higher values of H_2 conversion compared to CO conversion is attributed to the stochiometric ratio of H_2/CO taking the value 3 for producing methane, which then shifts to 2 in paraffin formation.

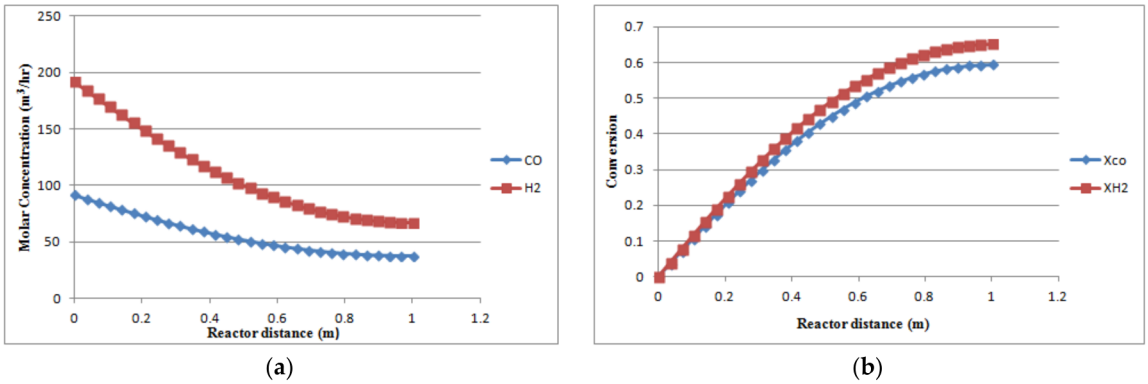

(**a**) (**b**)

Figure 12. The syngas variation on the reactor inside, (**a**) Molar concentration of CO and H_2; (**b**) CO and H_2 conversion.

The molar concentration of other FT species along the reactor height at three load conditions is also investigated as shown in Figure 13. It shows that all products increase with more or less the same intensity apart from naphtha (C_5–C_{10}) and diesel (C_{11}–C_{19}) which shift to lower values at higher syngas flow rate loads.

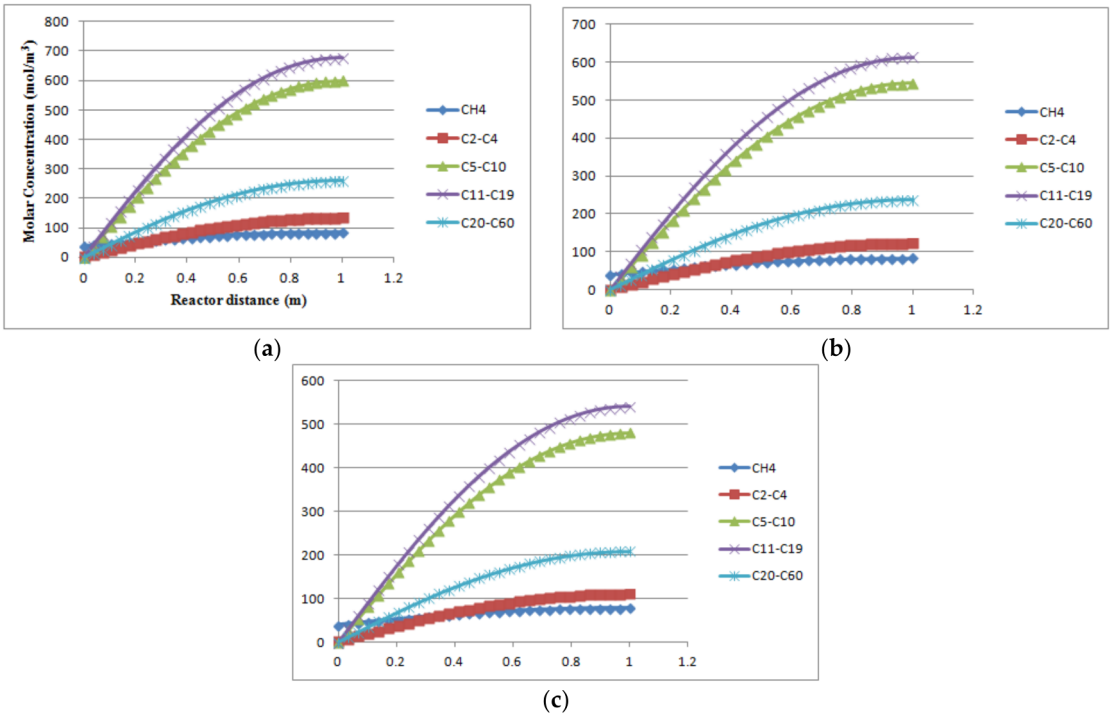

(**a**) (**b**)

(**c**)

Figure 13. The molar concentration of the FT products along the reactor bed at three load conditions: (**a**) T = 503 K, P = 20 bar, V_f = 3.5 m^3/h; (**b**) T = 503 K, P = 20 bar, V_f =5 m^3/h; (**c**) T = 503 K, P = 20 bar, V_f = 7.5 m^3/h.

Furthermore, Figure 14 illustrates the reduction of superficial gas velocity at three different loads of conditions based on the overall mass balance (Equation (11)).

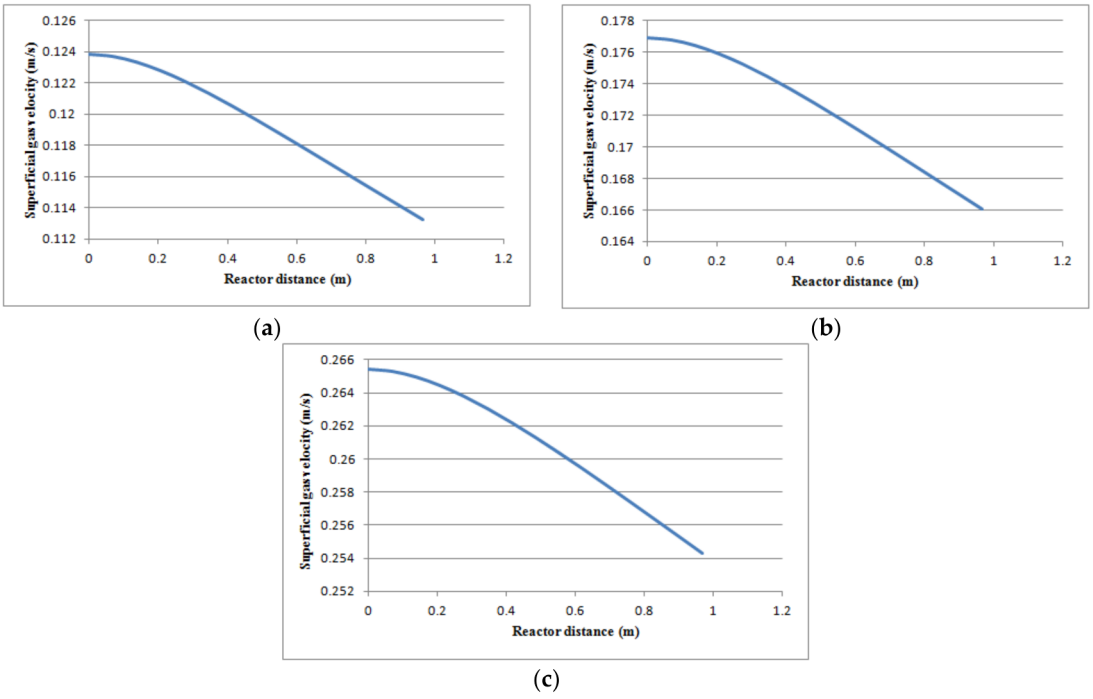

Figure 14. Reduction of superficial gas velocity as a function of reactor height at three different operating load conditions: (**a**) T = 503 K, P = 20 bar, V_f = 3.5 m^3/h; (**b**) T = 503 K, P = 20 bar, V_f = 5 m^3/h; (**c**) T = 503 K, P = 20 bar, V_f = 7.5 m^3/h.

5. Conclusions

A rigorous computer model for a lab-scale FT slurry reactor was developed to investigate flexible reactor operation. This flexibility was performed by a step-change of syngas flow rate load (3.5, 5, 7.5 m^3/h) in a low-temperature Fischer–Tropsch synthesis. It was found that the dynamic simulation is not only able to predict all Fischer–Tropsch components over the reactor bed but can also describe the behavior of superficial gas velocity as a sub-model using the overall gas mass balance.

The effect of a step-change volumetric syngas flow on the performance of FT slurry reactor was investigated. The results show that the temperature distribution of the slurry reactor remains constant under base load and change load conditions. It can be concluded that load change conditions do not have a negative influence on the temperature distribution inside the reactor and the presented dynamic model of the slurry reactor responds quite well to the load change conditions.

Acknowledgments: The authors acknowledge financial support by the Austrian government through the "Klima und Energiefonds" financed Project Winddiesel_klienIF within the "e!Mission.at" funding scheme. The project Winddiesel_klienIF is executed in cooperation with Energie Burgenland AG, Bilfinger SEBUR, Güssing Energy Technologies GmbH, Renewable Power Technologies Umwelttechnik GmbH, Energy & Chemical Engineering GmbH and the Institute of Chemical Engineering from TU WIEN.

Author Contributions: R.R., H.H. and G.W. prepared the materials and designed the experiments and S.S., R.R., S.B. and G.S. contributed to the paper writing.

Conflicts of Interest: The authors declare no conflict of interests.

Nomenclature

A_r (m^3)	Reactor cross sectional area
a (m^2 m^{-3})	Effective gas-liquid interfacial area per unit bed volume
C_i (mol/m^3)	Concentration of component i
C_{tot} (mol/m^3)	Total concentration of gaseous components
C_{tot}^L (mol/m^3)	Total concentration of liquid components
$D_{ax,L}$ (m^2/s)	Liquid phase axial dispersion coefficient
D_g (m^2/s)	Gas phase axial dispersion coefficient
D_t (m)	Reactor diameter
d_0 (m)	Gas distributor diameter
d_B (m)	Bubble diameter
g (m/s^2)	Acceleration due to gravity
H (m)	Reactor height
H_i (m_G^3 m_L^{-3})	Henry's solubility constant of gaseous component i
H_i^* (MPa. m^3/kmol)	Coefficient in Henry's law for gaseous component i
$-\Delta H_{s,i}$ (kJ/kmol)	Heat of solution for gaseous component i
K_l a (s^{-1})	Volumetric Mass transfer coefficient
$MW_{ave,L}$ (kg mol^{-1})	Average molecular weight of liquid components
P (Pa or bar)	Pressure
Pi,sat (bar)	Vapor pressure of component i
R (J mol^{-1} K^{-1})	Gas constant
R_{co} (mol kg_{cat}^{-1} s^{-1})	Carbon monoxide consumption rate
r_i (mol kg_{cat}^{-1} s^{-1})	Chemical reaction rate of component i
T (K)	Temperature
t (s)	Time
U_g (m/s)	Superficial gas velocity
U_l (m/s)	Liquid velocity
V_{cat} (m^3)	Volume of catalyst in column
V_f (m^3/h)	Volumetric gas flow rate
V_{gas} (m^3)	Volume of gas in column
V_{liquid} (m^3)	Volume of liquid in column
$V_L(0)$ (m/s)	Center-line liquid velocity
z (m)	Axial coordinate
Z	Compressibility factor, dimensionless
Greek Letters	
α	Chain growth probability factor, dimensionless
ε_g (m_G^3 m_R^{-3})	Gas holdup, dimensionless
ε_l (m_L^3 m_R^{-3})	Liquid holdup, dimensionless
ε_{cat} (m_{cat}^3 m_L^{-3})	Catalyst volume fraction
γ_i	Activity coefficient for component i, dimensionless
ρ_{cat} (kg/m^3)	Catalyst density
ρ_{sL} (kg/m^3)	Slurry density
μ_l (Pa.s)	Liquid viscosity
σ (N/m)	Surface tension
ρ_G (kg/m^3)	Gas density
ν (m^2/s)	Kinematic viscosity of phase
τ	Dimensionless time coordinate

Abbreviations

ADM-SBCD	Axial Dispersion Model- Single Bubble Class Diameter
ASF	Anderson-Sculz-Flory
CCU	Carbon Capture Unit
CPU	Central Processing Unit
FBR	Fixed Bed Reactor
FT	Fischer–Tropsch
GHG	Greenhouse Gas
MOL	Method Of Lines
ODE	Ordinary Differential Equation
PDE	Partial Differential Equation
PDEPE	Partial Differential Equations Parabolic Elliptic
RES	Renewable Energy Sources
SBCR	Slurry Bubble Column Reactor

Appendix A

Table A1. Average composition of Inlet/Outlet Gases under BL condition [12].

Inlet/Outlet Gas	N_2	CO_2	CH_4	C_2H_4	C_2H_6	CO	C_3H_6	C_3H_8	H_2
Syngas (vol. %)	4.6	24.2	8.4	2.5	0.3	19.1	~0	~0	40.1
Off-gas (vol. %)	7.0	39.0	14.4	0.1	4.5	12.1	~0	0.1	22.6

Table A2. Average composition of Inlet/Outlet Gases under CL condition [12].

Inlet/Outlet Gas	N_2	CO_2	CH_4	C_2H_4	C_2H_6	CO	C_3H_6	C_3H_8	H_2
Syngas (vol. %)	2.5	25.1	9.5	2.8	0.2	19.2	~0	~0	40.1
Off-gas (vol. %)	3.6	40.6	16.5	~0	5.0	11.7	~0	0.1	22.4

Appendix B

Table A3. Mass fraction of the FT products measured by off-line device [12].

Products	C_8	C_9	C_{10}	C_{11}	C_{12}	C_{13}	C_{14}	C_{15}	C_{16}
BL	0.0039	0.0072	0.012	0.0186	0.0271	0.0361	0.0442	0.0506	0.0536
CL	0.0095	0.0167	0.0238	0.0323	0.0405	0.0487	0.0555	0.0606	0.0624
Products	C_{17}	C_{18}	C_{19}	C_{20}	C_{21}	C_{22}	C_{23}	C_{24}	C_{25}
BL	0.0538	0.0524	0.0505	0.048	0.0454	0.0427	0.0395	0.0364	0.0334
CL	0.0604	0.0564	0.0498	0.0415	0.0333	0.0262	0.0206	0.0177	0.016
Products	C_{26}	C_{27}	C_{28}	C_{29}	C_{30}	C_{31}	C_{32}	C_{33}	C_{34}
BL	0.0307	0.0285	0.0265	0.0244	0.0229	0.0214	0.0193	0.0178	0.0158
CL	0.016	0.0161	0.0181	0.0202	0.0218	0.0227	0.0222	0.0213	0.0177
Products	C_{35}	C_{36}	C_{37}	C_{38}	C_{39}	C_{40}	C_{41}	C_{42}	C_{43}
BL	0.0143	0.0127	0.0115	0.0107	0.0098	0.0088	0.0081	0.0072	0.0063
CL	0.0135	0.0128	0.0129	0.0126	0.0122	0.011	0.0103	0.0094	0.0083
Products	C_{44}	C_{45}	C_{46}	C_{47}	C_{48}	C_{49}	C_{50}	C_{51}	C_{52}
BL	0.0059	0.0053	0.0046	0.0043	0.0039	0.0034	0.0031	0.0028	0.0025
CL	0.0075	0.0065	0.0058	0.0049	0.0043	0.0036	0.0032	0.0027	0.0022
Products	C_{53}	C_{54}	C_{55}	C_{56}	C_{57}	C_{58}	C_{59}	C_{60}	
BL	0.0022	0.002	0.0018	0.0016	0.0014	0.0012	0.0011	0.0009	
CL	0.0018	0.0015	0.0013	0.0011	0.0009	0.0007	0.0006	0.0005	

BL: Base Load condition (V_f =5 m^3/h). CL: Change Load condition (V_f =3.5, 7.5 m^3/h).

References

1. Varone, A.; Ferrari, M. Power to liquid and Power to gas: An option for the German *Energiewende*. *J. Renew. Sustain. Energy Rev.* **2015**, *45*, 207–218. [CrossRef]
2. Eilers, H.; González, M.I.; Schaub, G. Lab-scale experimental studies of Fischer–Tropsch kinetics in a three-phase slurry reactor under transient reaction conditions. *Catal. Today* **2015**, *275*, 164–171. [CrossRef]
3. König, D.H.; Freiberg, M.; Dietrich, R.-U.; Wörner, A. Techno-economic study of the storage of fluctuating renewable. *Fuel* **2015**, *159*, 289–297. [CrossRef]
4. Cinti, G.; Baldinelli, A.; di Michele, A.; Desideri, U. Integration of Solid Oxide Electrolyzer and Fischer-Tropsch: A sustainable pathway for synthetic fuel. *Appl. Energy* **2016**, *162*, 308–320. [CrossRef]
5. Maitlis, P.M.; de Klerk, A. *Greener Fischer Tropsch Process for Fuels and Feedstocks*; John Wiley & Sons: Weinheim, Germany, 2013; pp. 40–58. ISBN 9783527326051.
6. Gross, P.; Rauch, R.; Hofbauer, H.; Aichering, C.; Zweiler, R. Winddiesel Technology—An alternative to power to gas systems. In Proceedings of the 23rd European Biomass Conference and Exhibition, Vienna, Austria, 1–4 June 2015.
7. Gonzalez, M.I. Gaseous Hydrocarbon Synfuels from H_2/CO_2 based on Renewable Electricity-Kinetics, Selectivity and Fundamentals of Fixed-Bed Reactor Design for Flexible Operation. Ph.D. Thesis, Karlsruher Institute für Technologie (KIT), Karlsruher, Germany, 2016.
8. Gonzalez, M.I.; Eilers, H.; Schaub, G. Flexible Operation of Fixed bed Reactors for a Catalytic Fuel Synthesis-CO_2 Hydrogenation as Example Reaction. *Energy Technol.* **2016**, *4*, 90–103. [CrossRef]
9. Lucero, A. *Improved Fischer Tropsch Slurry Reactors*; Worked Performed under Cooperative Agreement JSR Task 26 Under DE-FC26-98FT40323; PowerEnerCat, Inc.: Lakewood, CO, USA, 2009.
10. Sehabiague, L.; Morsi, B.I. Modeling and Simulation of Fischer-Tropsch Slurry Bubble Column Reactor Using different kinetic rate expressions for Iron and Cobalt Catalysts. *Int. J. Chem. React. Eng.* **2013**, *11*, 309–330. [CrossRef]
11. Sauciuc, A.; Abosteif, Z.; Weber, G.; Potetz, A.; Rauch, R.; Hofbauer, H.; Schaub, G.; Dumitrescu, L. Influence of operating conditions on the performance of biomass-based Fischer-Tropsch synthesis. *Biomass Convers.* **2012**, *2*, 253–263. [CrossRef]
12. Abulmfalfel, R. Winddiesel: Power to Liquids Assisted by Biomass Steam Gasification. Master's Thesis, Karlsruhe Institute of Technology, Karlsruher, Germany, March 2017.
13. Novica, R.; Al-Dahhan, M.H.; Duduković, M.P. Dynamic modeling of slurry bubble column reactors. *Ind. Eng. Chem. Res.* **2005**, *16*, 6086–6094. [CrossRef]
14. De Swart, J.W.A.; Krishna, R. Simulation of transient and steady state behavior of a bubble column slurry reactor for Fischer-Tropsch synthesis. *Chem. Eng. Process.* **2002**, *41*, 35–47. [CrossRef]
15. Hooshyar, N.; Fatemi, S.; Rahmani, M. Mathematical Modeling of Fischer-Tropsch Synthesis in an industrial Slurry Bubble Column. *Chem. React. Eng.* **2009**, *7*. [CrossRef]
16. Maretto, C.; Krishna, R. Modelling of a bubble column slurry reactor for Fischer-Tropsch synthesis. *Catal. Today* **1999**, *52*, 279–289. [CrossRef]
17. Sehabiague, L.; Lemoine, R.; Behkish, A.; Heintz, Y.J.; Sanoja, M.; Oukaci, R.; Morsi, B.I. Modeling and optimization of a large-scale slurry bubble column reactor for producing 10,000 bbl/day of Fischer–Tropsch liquid hydrocarbons. *J. Chin. Inst. Chem. Eng.* **2008**, *39*, 169–179. [CrossRef]
18. Krishna, R.; Urseanu, M.I.; van Baten, J.M.; Ellenberger, J. Liquid phase dispersion in bubble columns operating in the churn-turbulent flow regime. *Chem. Eng. J.* **2000**, *78*, 43–51. [CrossRef]
19. Ian, C.Y.; Satterfield, C.N. Intrinsic kinetics of the Fischer-Tropsch synthesis on a cobalt catalyst. *Energy Fuels* **1991**, *5*, 168–173. [CrossRef]
20. Baliban, R.C.; Elia, J.A.; Floudas, C.A. Toward Novel Hybrid Biomass, Coal, and Natural Gas Processes for Satisfying Current Transportation Fuel Demands, 1: Process Alternatives, Gasification Modeling, Process Simulation, and Economic Analysis. *Ind. Eng. Chem. Res.* **2010**, *49*, 7343–7370. [CrossRef]
21. Song, H.-S.; Ramkrishna, D.; Trinh, S.; Wright, H. Operating Strategies for Fischer-Tropsch Reactors: A Model-Directed Study. *Korean J. Chem. Eng.* **2004**, *21*, 308–317. [CrossRef]
22. Joseph William, P. *A Fischer-Tropsch Synthesis Reactor Model Framework for Liquid Biofuels Production*; Sandia National Laboratories: Livermore, CA, USA, 2012.

23. Watson, L.A. Solar-Boosted Biomass-to-Liquid (BtL) Process Modelling. Bachelor Thesis, Australian National University, Canberra, Australia, 2011.
24. Marano, J.J.; Holder, G.D. Characterization of Fischer-Tropsch liquids for vapor-liquid equilibria calculations. *Fluid Phase Equilib.* **1997**, *138*, 1–21. [CrossRef]
25. Shah, Y.T.; Dassori, C.G.; Tierney, J.W. Multiple steady states in non-isothermal FT slurry reactor. *Chem. Eng. Commun.* **1990**, *88*, 49–61. [CrossRef]
26. Marano, J.J.; Holder, G.D. General equation for correlating the thermophysical properties of *n*-paraffins, *n*-olefins, and other homologous series. 2. Asymptotic behavior correlations for PVT properties. *Ind. Eng. Chem. Res.* **1997**, *36*, 1895–1907. [CrossRef]
27. Lau, R.; Peng, W.; Velazquez-Vargas, L.G.; Yang, G.Q.; Fan, L.S. Gas-liquid mass transfer in high-pressure bubble columns. *Ind. Eng. Chem. Res.* **2004**, *43*, 1302–1311. [CrossRef]
28. Loipersböck, J.; Weber, G.; Gruber, H.; Kratky, J.; Capistrano, R.; Hofbauer, H.; Rauch, R. Upscaling and operation of a biomass-derived Fischer-Tropsch pilot plant producing one barrel per day. In Proceedings of the 25th European Biomass Conference and Exhibition, Stockholm, Sweden, 12–15 June 2017; pp. 1088–1093. [CrossRef]
29. Behkish, A. Hydrodynamic and Mass Transfer Parameters in Large-Scale Slurry Bubble Column Reactors. Ph.D. Thesis, University of Pittsburgh, Pittsburgh, PA, USA, 2005.
30. Krishna, R.; Sie, S.T. Design and Scale up of the Fischer Tropsch Bubble Column Slurry Reactor. *Fuel Process. Technol.* **2000**, *64*, 73–105. [CrossRef]
31. Krishna, R. A Scale-up Strategy for a Commercial Scale Bubble Column Slurry Reactor for Fischer-Tropsch Synthesis. *Oil Gas Sci.* **2000**, *4*, 359–393. [CrossRef]
32. Eric, H.; Iglesia, E. Slurry Bubble Column (C-2391). U.S. Patent No. 5,348,982, 20 September 1994.